High Brightness ZnS and GaN Electroluminescent Devices Using PZT Thick Dielectric Layers

Chanaka Munasinghe, *Student Member, IEEE*, Jason Heikenfeld, *Member, IEEE*, Robert Dorey, Roger Whatmore, *Member, IEEE*, Jeffrey P. Bender, John F. Wager, *Senior Member, IEEE*, and Andrew J. Steckl, *Fellow, IEEE*

***Abstract*—An improved thick dielectric (TD) layer for inorganic electroluminescent (EL) display devices has been achieved through a composite high-κ dielectric sol-gel/powder route. This composite TD film results in a luminance improvement (up to $10\times$) in these TDEL devices with Eu-doped GaN and Mn-doped ZnS phosphor layers. The use of a composite TD film, composed primarily of lead–zirconate–titanate (PZT), results in a significantly higher charge ($> 3\ \mu C/cm^2$) coupling to the phosphor layer. Furthermore, the reduction in porosity of the TD has improved the homogeneity of electric field applied to the phosphor layer, resulting in a steeper luminance–voltage slope. The reduction in porosity has also decreased the diffuse reflection of the TD, which when pigmented, exhibits a diffuse reflectivity of $< 2\%$ resulting in high display contrast. High luminance levels of up to 3500 cd/m^2 have been achieved from the ZnS:Mn TDEL devices and 450 cd/m^2 from GaN:Eu devices. A detailed analysis of the electrical steady-state time-varying characteristics has shown that the electrical performance of TDELs is very similar to TFELs in spite of the physical asymmetry in the device structure. These results demonstrate that three critical requirements for practicality of the TDEL approach (formation on standard display glass, low reflectivity, and electric field homogeneity) can be obtained by careful selection and design of the device materials, fabrication process and device structure.**

***Index Terms*—Electrical characterization, electroluminescent device, GaN:RE, luminance, lead zirconate titanate (PZT), thick dielectric (TD), ZnS:Mn.**

I. Introduction

THE PUSH toward flat panel displays has been led primarily by liquid crystal display and plasma display panel technologies. Other display technologies include field emission displays [1], [2], organic light emission diodes [3], thin-film electroluminescent displays (TFEL) and thick dielectric electroluminescent displays (TDEL) [4]. After three decades of research on these intriguing TFEL devices [5], [6], monochrome (amber) TFEL displays are currently commercially available [7] and full-color TDEL displays are being developed [8]. The development of EL device technology is driven by several requirements: high luminance, simple fabrication methods such as screen-printing [9] which can reduce the manufacturing costs, and higher contrast ratios [10] which enable the display to perform equally well under strong lighting conditions.

We have been investigating [11] TDEL devices utilizing the visible light emission from lanthanide (rare-earth) and transition metal elements. The host material strongly influences the radiative emission probability of the rare earth atoms, but not the emission wavelength. Wide bandgap host material systems such as GaN are preferred due to their low RE emission thermal quenching and excellent high-field carrier transport properties [12]. Materials and device aspects of GaN:RE ELDs can be found in a recent review article [13].

Other phosphor systems (oxides, sulfides) are also of interest for developing high luminance TDEL devices. Zinc sulfide is a widely studied phosphor host material which can be most efficiently doped with the transition metal Mn. Mn-doped ZnS has a relatively broad emission band [14]–[16] with the peak maximum at ~ 585 nm for Mn concentrations not exceeding 0.5–1 wt. %. Our interest in the ZnS:Mn material system is not only as a yard stick for the novel GaN:RE material system but also for high brightness monochrome displays.

In this paper, we present an electro-optical analysis of high luminance results for TDEL devices using a novel composite TD layer. Device characterization is performed for both full color (GaN:RE) and monochrome (ZnS:Mn) phosphor systems. The novel TD [17] is composed of a composite lead zirconate titanate (PZT) sol-gel and powder slurry which can be spin-coated, dip-coated, or screen-printed and sintered to form a film which possesses a very high dielectric constant of $\varepsilon_r \sim 1000$. We present a systematic assessment of time-variant charge, voltage, current, and phosphor field characteristics of TDEL devices. Other device characterization methods include external charge versus voltage (Q–V), internal charge versus phosphor field (Q–F_p), capacitance versus voltage (C–V), and maximum charge versus maximum applied voltage (Q_{max}–V_{max}) analysis [18]–[21]. These methods will be analyzed with respect to GaN:Eu and ZnS:Mn TDEL devices.

II. Device Structure and Operation

The EL phosphors are operated most efficiently at or near their electrical breakdown voltage (high field$\sim$ MV/cm). AC EL devices have been developed utilizing a thin dielectric layer on the electroluminescent thin film. This method creates the

Manuscript received June 16, 2004; revised November 8, 2004. The work at Cincinnati was supported by the U.S. Army Research Laboratory. R. Dorey's work was supported by a Royal Academy of Engineering/EPSRC Postdoctoral Research Fellowship. The review of this paper was arranged by Editor J. Hynecek.

C. Munasinghe and A. J. Steckl are with the Nanoelectronics Laboratory, University of Cincinnati, Cincinnati, OH 45221-0030 USA (e-mail: a.steckl@uc.edu).

J. Heikenfeld is with Extreme Photonix, LLC, Cincinnati, OH 45219-2374 USA.

R. Dorey and R. Whatmore are with Cranfield University, Cranfield, U.K.

J. P. Bender is with Intel Corporation, Aloha, Oregon USA.

J. F. Wager is with the School of Electrical Engineering and Computer Science, Oregon State University, Eugene, Oregon 97331-3211 USA.

Digital Object Identifier 10.1109/TED.2004.842542

high field needed for the thin EL phosphor operation by allowing reversible (current limited) electrical breakdown.

Proper thin dielectric selection must satisfy several criteria. First, the dielectric permittivity (ε_r) and breakdown field ($E_{\rm br}$) must be sufficiently high to efficiently and reliably couple the applied device voltage to the phosphor layer. This first requirement is satisfied by selecting dielectrics which can provide a charge capacity equal to or greater than that of common phosphors: capacitance of $\sim$ 10 nF/cm^2, $E_{\rm br} \sim 1$ MV/cm, $\varepsilon_r \sim$ 8–12. Generally, the permittivity and breakdown field of dielectric materials do not increase together [22], leading to candidate dielectrics having properties ranging from $E_{\rm br} \sim$ 4–8 MV/cm and $\varepsilon_r \sim 4$–$10's$, to $E_{\rm br} \sim 0.1$ MV/cm and $\varepsilon_r \sim 100's$–$1000's$. Therefore, it is customary to consider the product of the permittivity and breakdown field as a figure of merit of a dielectric material. However, very few thin-film dielectrics meet two additional requirements for EL usage: a) proper interfacial sheet charge properties with the phosphor; and b) nonpropagating, self-healing breakdown mode. Historically, this has limited practical thin-film dielectrics [23] to providing only moderate capacitance, such as SiON ($\sim$ 20 nF/cm^2) and Al_2O_3:TiO_2 ($\sim$ 30 nF/cm^2). Furthermore, it is difficult to eliminate the existence of particulates, film roughness, and pinholes in thin-film dielectrics, which in turn lowers their breakdown field below the intrinsic level. Such difficulties in thin dielectric implementation only intensify with increases of the overall device area.

The AC-TDEL device is designed to eliminate the limitations of thin-film dielectrics while maintaining the virtues of a TFEL device [9]. The TDEL device consists of a TD film layer and several thin-film stacks arranged in a metal–insulator–semiconductor–insulator–metal structure. Typically, the "standard" structure AC-TDEL shown in Fig. 1 is built on a transparent glass substrate, through which light will reach the viewer. The bottom electrode is a $\sim$ 200-nm-thick transparent conductive electrode such as zinc aluminum oxide (ZNA), or indium tin oxide (ITO) layer. Next, a thin dielectric layer is deposited on top of the transparent electrode. In the case of the GaN-based TDEL devices the thin dielectric layer is typically a $\sim$ 100 -nm-thick strontium titanate (STO) with a relative permittivity of $\varepsilon_r \sim 140$. The STO layer acts as both as a buffer layer assisting the growth of the GaN phosphor layer as well as an interface charge trapping layer for the GaN TDEL device. In the case of the ZnS:Mn TDEL device the thin dielectric layer is typically a sputtered 100-nm-thick barium titanate (BTO) with a relative permittivity $\varepsilon_r \sim 500$. In this case the BTO layer functions mainly as an interface charge-trapping layer. We have found that both BTO and STO thin dielectric layers perform equally well as thin charge trapping dielectric layers in the TDEL device. The phosphor layer is deposited next. An upper thin dielectric film then encapsulates the phosphor layer. The choice of dielectric material on either side of the phosphor is made based on considerations of charge homogeneity on both phosphor-dielectric interfaces during opposite polarities of the driving ac waveform. This is followed by a coupling dielectric layer, typically a 250-nm-thick alumina layer (further explained in the next section). The alumina layer is covered by the TD film, which is characteristic of the ACTDEL device.

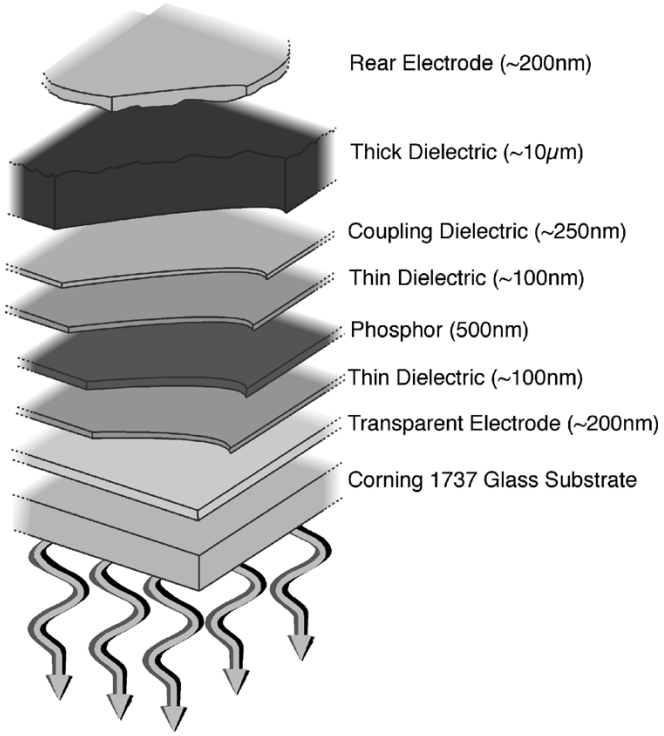

Fig. 1. TDEL device structure.

The TD film allows higher charge coupling across the device. Finally, the rear opaque metal electrode is deposited. Typically, the rear electrode is made of aluminum, which possesses a self-healing characteristic that contains the breakdown process at localized sites.

Device operation [24] involves charge transport and charge interaction within both phosphor and dielectric layers. The charge traveling across the phosphor material results in either impact excitation or ionization of the luminescent centers, or charge scattering and energy transfer to the phosphor host atoms, host defects, or to other charge carriers. Luminescent centers in excited states return to their ground state by either emission of photons or through nonradiative processes.

In an AC-TDEL device driven at ac voltages corresponding to fields across the phosphor below the breakdown value, the insulating and phosphor layers are effectively capacitors in series. In an ideal device structure, the dielectric layers maintain their capacitive qualities when the phosphor layer experiences breakdown. Once the phosphor breakdown field is exceeded, the purely capacitive behavior of the phosphor layer is no longer observed. This is the threshold voltage for charge flow across the phosphor. The phosphor breakdown originates with the tunneling of electrons from the phosphor-insulator interface in the negatively biased side of the device. The onset of electron injection is very rapid due to the homogeneous ~ 1 eV charge trap depth at the phosphor-dielectric interface. Injected carriers subsequently gain sufficient energy in the high phosphor electric field ($\sim$ 1–2 MV/cm) and in turn excite the luminescent centers. Given an electric field of 1 MV/cm, a ballistic electron could gain adequate excitation energy (> 2.0 eV) within an accelerating path [25] length of only $\sim$ 20 nm. Theoretically, for a phosphor layer thickness of $\sim$ 500 nm, ballistic transit would result in 25 impact excitations per injected electron. The excited

luminescent centers return to the ground state through emission of a photon of wavelength characteristic to the nature of the luminescent centers or through nonradiative processes such as the emission of a phonon. Naturally, for high efficiency luminescent devices, radiative relaxation (photon emission) is necessary. Assuming loss-free electron transport through the phosphor and maximum energy not exceeding the host impact ionization energy, a very steep luminance–voltage slope can result from strong host impact ionization (avalanching). A primary challenge to blue EL phosphors is to achieve strong avalanching, which however has an onset of ~ 3 eV, allowing for blue lumophor excitation. GaN has superior electron transport properties [26] that allow the electrons to be heated by the electric field to high energies, required to excite blue lumophores. However, even though this phenomenon is readily observed [27] in GaN on silicon substrates (dc devices), strong blue emission from GaN on glass substrates (ac device) has not yet been demonstrated. Possible reasons for this include: poor dielectric-phosphor interface properties which lead to shallow electron trapping with premature emission (prethreshold), loss in electron energy due to high point defect concentration in GaN layers grown on amorphous substrates. Upon reaching the opposite (anodic) phosphor-insulator interface, electrons are captured by the many electron traps at the interface. A fraction of the generated photons are out coupled and reach the viewer's eyes. The fraction out-coupled is approximately equal to $1/4n^2$, where n is the refractive index of the medium in which the photons are emitted (~ 2.4 for ZnS, ~ 2.2 for GaN).

III. Device Fabrication

Low-cost, high-throughput film deposition techniques are used for fabrication of the TDEL device. Typically, the "standard" TDEL structure (Fig. 1) is built on a transparent industrial grade Corning 1737 glass substrate. The bottom ITO electrode is either hot- or warm-sputtered and annealed at 450 °C for 10 min in nitrogen ambient. This enables the ITO films to be $> 90\%$ transparent to visible wavelengths (400–700 nm) and reduces the sheet's resistance to 15–20 Ω/square. Next, the thin dielectric is sputter deposited on top of the ITO film: STO for GaN TDEL devices and BTO for ZnS TDEL devices. Both BTO and STO perform well as thin charge trapping dielectric layers in the TDEL device, but they differ when it comes to functioning as a buffer layer for phosphor growth. The phosphor layers are deposited by either sputtering or molecular beam epitaxy (MBE). For the GaN TDEL devices the phosphor is deposited using a Riber 32 solid source MBE system. GaN:RE phosphors are typically deposited at ~ 600 °C, which is adequately below the strain point (666 °C) of the Corning 1737 glass substrate. We have previously shown [28] that the optimum RE concentrations in GaN host is around 1at. %. The ZnS:Mn phosphor is deposited using a Denton Vacuum Discover 18 Magnetron sputtering system. The phosphor material is sputtered from a single ZnS:MnS target (0.6% MnS) at ~ 200 °C substrate temperature. The ZnS:Mn phosphor layer undergoes a 500–600 °C post sputtering anneal for efficient incorporation of the Mn atoms into the ZnS host lattice. A thin alumina layer is deposited on the phosphor to enhance both electrical and physical coupling between the thick and thin films. In addition, the alumina layer acts as a protective diffusion barrier against oxygen and organics produced during TD sintering at ~ 650 °C.

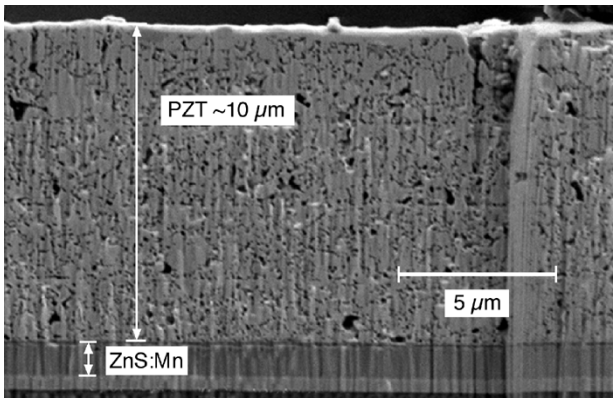

Fig. 2. SEM microphotograph of TDEL device cross section.

A novel process is utilized for TD deposition. Fig. 2 contains a scanning electron microscope (SEM) photomicrograph of the AC-TDEL device. The TD layer takes up most of the device cross section. The TD layer is deposited using a composite sol-gel technique whereby PZT (PZ26, Ferroperm) ceramic powder was mixed with a sol (metal–organic PZT precursor) and a dispersant (KR55, Kenrich Petrochemicals) to yield a slurry, which was deposited on the substrate. Subsequent firing converted the sol to an oxide ceramic, which bound the ceramic powder together and to the substrate.

The sol was produced [17] using lead acetate (Fisher), zirconium propoxide (Aldrich), titanium isopropoxide (Aldrich), manganese acetate (Aldrich), antimony ethoxide (Inorgtech), and niobium ethoxide (Inorgtech). The composition of the sol was designed to yield a PZT oxide ceramic of comparable composition to that of PZ26.

The composite slurry was produced by mixing the PZT powder and sol in a ratio of 1.5-g powder to 1 ml sol. A dispersant (2 wt% with respect to PZT powder mass) was added to stabilize the slurry. The films were deposited by spin coating where the substrate was coated with the composite slurry prior to spinning at 2000 rpm for 30 s . The film was then dried at 200 °C for 60 s to remove the solvent and pyrolyzed at 450 °C for 15 s to convert the sol to an amorphous PZT ceramic. To further increase the density (and hence relative permittivity) of the composite film, sol was infiltrated into the film. The system was then again spun and subjected to thermal treatments at 200 °C and 450 °C. This infiltration process was repeated a total of four times. To attain a 10-μm-thick PZT film a total of four composite layers were deposited, each subjected to four infiltration treatments. Once the required thickness of PZT had been deposited the films were subjected to a final crystallization treatment at 650 °C for 30 min designed to develop the ferroelectric perovskite crystal phase within the PZT material. The final product is a highly dense TD layer of high relative permittivity $\varepsilon_r > 1000$ and capacitance of > 40 nF/cm^2. Finally, the aluminum rear electrode was deposited on to the device using standard sputtering techniques.

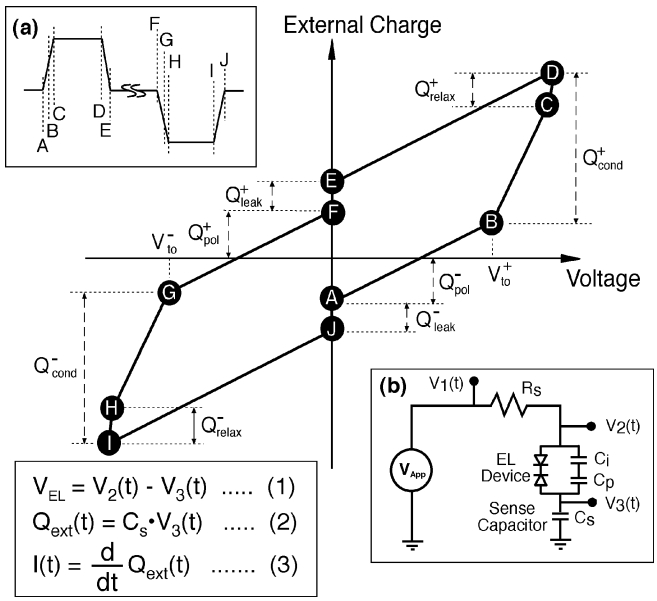

Fig. 3. Theoretical external charge–voltage plot of an ACTDEL device. Inserts: (a) bias pulse waveform; (b) Sawyer–Tower bias circuit.

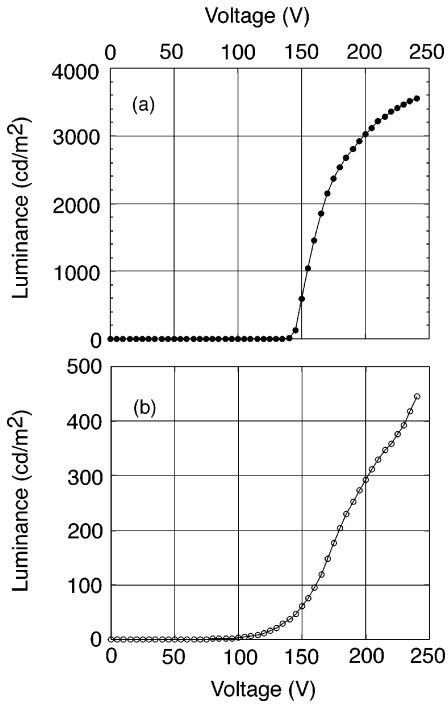

Fig. 4. Luminance–voltage characteristics for TDEL devices operated at 1 kHz: (a) ZnS:Mn; (b) GaN:Eu.

IV. Device Electro-Optical Characterization

Since the TDEL devices are voltage modulated high field devices, the most widely utilized electrical characterization technique for the devices is the dependence of external charge on applied voltage. This relationship reveals the charge transfer characteristics within an entire voltage cycle. Furthermore, the external charge–voltage relationship gives insight on the relationship between internal phosphor field and internal charge.

The test devices are circular dots with an emitting area of ~ 0.02 cm^2. The waveform used for electrical characterization of the TDEL devices is a bipolar-pulsed waveform of 1 kHz as depicted in insert (a) to Fig. 3. The pulse waveform has rise and fall times of 5 μs and a plateau of 30 μs. The bipolar pulse waveform was chosen since it is similar to the waveform used to drive commercial displays. The Sawyer–Tower [29] electrical circuit was employed for the charge–voltage measurements. The circuit consists of a series resistor and a series capacitor (sensor capacitor), as shown in insert (b) to Fig. 3. The characteristics of GaN:Eu and ZnS:Mn ACTDEL devices are discussed in detail in the following subsection of this paper.

A. Device Luminance–Voltage

The high brightness or luminance of the GaN:Eu and ZnS:Mn TDEL devices with 0.5-μm phosphor and PZT TD layers is seen in Fig. 4. The GaN:Eu and ZnS:Mn TDEL devices operated at 1 kHz reach a maximum brightness of 450 and 3350 cd/m^2 at 240 V. Luminance efficiency levels of $\sim$ 1.6 lm/W and $\sim$ 0.05 lm/W have been achieved for ZnS:Mn and GaN:Eu TDEL devices, respectively. The GaN:Eu device has chromaticity coordinates of $x = 0.6842$ and $y = 0.3157$, while the ZnS:Mn device has coordinates of $x = 0.5340$ and $y = 0.4654$. The x and y coordinates correspond to the 1931 Commission International d'Eclairage chromaticity diagram. In the GaN:Eu we can see a 10 $\times$ improvement in the luminance with the PZT TD layer, whereas in the ZnS:Mn TDEL device a 3 $\times$ increase in the luminance is measured. This implies that phosphor optimization in the GaN:Eu TDEL is also accountable for this increase in the brightness (from 3 $\times$ given by the PZT film to total of 10 $\times$ improvement). It is important to point out that, even though the impurity scattering by point defects in GaN is generally rather low compared to intervalley scattering and band-to-band impact ionization, we believe that for GaN:RE on glass substrates the impurity scattering due to reduced crystallinity (point defects) results in the cooling of the high energy electrons. The PZT TD layer is significantly more dense and more uniform than other dielectric materials, resulting in a more uniformly intimate interface with the phosphor layer. This contributes greatly to the sharp turn-on of the device. If the TD-phosphor interface is nonuniform (with air gaps), then the resulting high field points at localized regions in the device cause premature breakdown in the phosphor. Premature breakdown at localized regions leads to uneven luminance levels within the device [20]. It is important to note that both devices possess high luminance–voltage slopes. The luminance–voltage slope is directly proportional to the device efficiency, thus a high slope is desirable. The GaN:Eu TDEL device exhibits a luminance–voltage slope of 5.2 cd/(m^2-V) at around 150-V bias. The ZnS:Mn TDEL device shows a luminance–voltage slope of 60 cd/(m^2-V) around the 150-V threshold voltage. The shallow rise in the luminance above threshold in GaN:Eu TDEL device is mainly due to prethreshold conduction in the GaN phosphor due to insulator-phosphor interface irregularities. A steeper luminance–voltage slope is preferred for multiplex pixel addressing in flat panel displays. This is because a small increment in the modulation voltage on a selected pixel leads to a high brightness "on" pixel while the nonaddressed pixels maintain their off status, thus achieving high level of contrast.

B. Electrical Characterization

The electrical analysis was performed for the case when the AC-biased device has reached stable (i.e., steady-state) operation. We have used the approach and nomenclature developed by Wager [18] *et al.* for the analysis of the electrical characteristics of TFEL devices. Voltages V_2 and V_3 measured across the ACTDEL device (see insert (b) in Fig. 3) are used to calculate the electrical properties of the device. The equations used to calculate the external applied device voltage $V_{\rm EL}$, external charge of the device ($Q_{\rm ext}(t)$) and the time-variant current ($I(t)$) are illustrated in the insert of Fig. 3. It is important to point out that the charge transported across the phosphor layer is identical to the charge built up at the sensor capacitor only when the conduction current density in the phosphor is large enough to consider the phosphor capacitance to be shunted out of the circuit. Using this measurement setup, the desired measurement of charge transferred across the phosphor, $Q(t)$, is not measured directly, but calculated according to the relationship

$$Q(t) = \frac{(C_i + C_p)}{C_i} C_s V_3(t) - C_p \left[V_2(t) - V_3(t)\right] \qquad (1)$$

where C_i and C_p are the insulator and phosphor capacitance values, respectively. It is important to recognize that the device external charge measured on a TDEL device consists of union of capacitive displacement charge ($Q_{\rm disp} = C_p V_p$) and actual conduction charge across the phosphor layer. In other words, it is worthy to note that the difference between the $Q_{\rm ext}(t)$ and $Q(t)$ involves rescaling and subtracting the displacement charge.

The raw data for Q–F_p calculations are gathered from the Sawyer–Tower circuit. The field across the phosphor is calculated as follows:

$$F_p = \frac{1}{d_p}\left\{\frac{C_s V_3(t)}{C_i} - \left[V_2(t) - V_3(t)\right]\right\} \qquad (2)$$

where C_s and C_i, are the sensor and insulator capacitances, and d_p is the phosphor thickness. It is important to note that the accuracy of the field assessment requires that C_s, C_i, and d_p be determined accurately. This equation assumes that there is no space charge generation within the phosphor. In practice, this is not the case for many EL devices. Even if there is dynamic space charge generation (2) will be true, but in that case it is important to realize that the electric field calculated is rather the average field across the phosphor.

1) Steady-State Time-Variant Electrical Characteristics: The time-resolved electrical characterization of the ZnS:Mn and GaN:Eu TDEL devices is shown in Figs. 5 and 6, respectively. Fig. 7 contains the external charge–voltage (Q–V) plots obtained with the same bias waveform.

Electrical characterization is referenced to alphabetically labeled events for a bipolar trapezoidal pulse, which is shown in insert (a) of Fig. 3 (in an idealized form) and in Fig. 5(a) as a measured waveform. For all data, the devices experience multiple bias cycles prior to data measurement, which results in an offset of voltages and an initial charge leakage due to induced built-in potential across the phosphor layer. The time-variant characterization for ZnS:Mn TDEL shown in Fig. 5 begins with

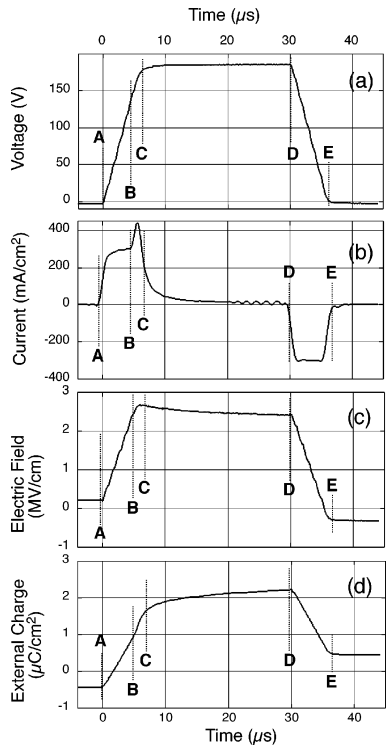

Fig. 5. ZnS:Mn TDEL time-variant characteristics.

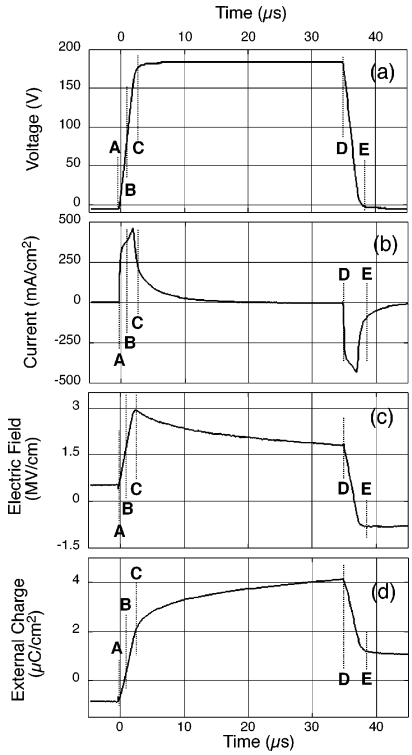

Fig. 6. GaN:Eu TDEL time-variant characteristics.

the device at ground after several such cycles of operation. As the applied pulse increases from A to B, the device is below the threshold voltage. Therefore, the electric field is not sufficient for the electrical breakdown of the phosphor and emission of light. During this period there is only a displacement current

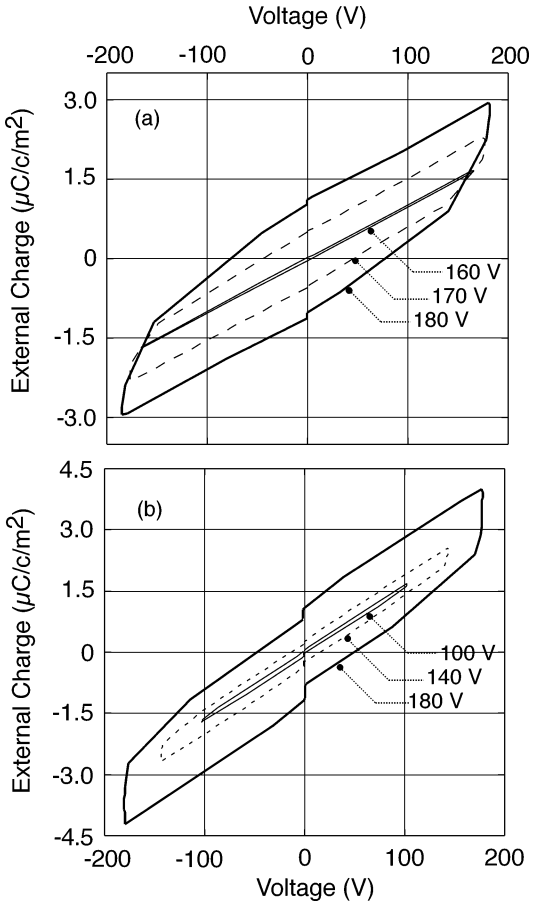

Fig. 7. External charge–voltage plots for TDEL devices: (a) ZnS:Mn and (b) GaN:Eu.

across the device. This is the dielectric displacement current resulting from $I = C(dV/dt)$ relationship, where C is the capacitance of the entire stack. Once the applied voltage has reached point B, the device has reached its threshold voltage (phosphor breakdown). Ideally, at B, the charge trapped at the phosphor-insulator interface begins to flow across the phosphor, and thus the phosphor field is "clamped." However, for our devices we have not been able to observe this effect. The fact that the phosphor is not going through a complete breakdown due to defects (in other words, it behaves not as a perfect capacitor, but a capacitor in parallel with a resistor) could be the reason for observing the clamping effect. Due to charge transport across the phosphor, current is initiated at point B. The conduction current is superimposed on to the displacement current during this period of time [Fig. 5(b)]. The flow of charge across the TDEL device will be at a higher rate once the phosphor electric field is clamped as seen in a sharp increase in the slope at point B on Fig. 5(d). As the applied voltage is constant from point C to D, a relaxation in the electric field across the phosphor occurs due to continued charge transfer ("relaxation" charge). Finally, the period D-E is the falling edge of the waveform where the applied voltage decreases to zero and the residual built-in charge and field are measured as shown in Figs. 5 and 6. A similar situation occurs during the opposite polarity pulse, where the charge transfer will be in the opposite direction from the above. It is clearly seen that conduction current is initiated at point B. During A-B only displacement current is present in the ZnS:Mn ACTDEL [Fig. 5(b)], implying a strong charge trapping at the phosphor-insulator interface.

The GaN ACTDEL does not show a very sharp increasing conduction current at the device turn on point [point B in Fig. 6(a) and (b)]. Charge leakage across the phosphor below threshold, poor charge trapping at the interfaces and smaller amount of space charge generation in GaN devices are probable reasons for slow rise in the luminance around threshold. Further tests are being conducted for verification of this hypothesis and development in interface charge trapping capabilities in GaN:Eu ACTDEL devices.

The time-variant phosphor field data [Figs. 5(c) and 6(c)] are often used to investigate the detailed dynamics associated with the field clamping, trailing edge emission, and field relaxation. Once the device is biased, when the applied voltage keeps on increasing from A to B there will be an accumulation of charge on the device [Figs. 5(d) and 6(d)] which in turn will result in an increasing electric field [Figs. 5(c) and 6(c)]. The phosphor field curve for the ZnS:Mn TDEL possesses a brief period at which the field is nearly constant with time (B to C). This constant field, which arises at the peak of the field, is the "steady-state" field. The steady-state phosphor field $F_{\rm ss}$ is independent of the maximum applied voltage for a TDEL device. The steady-state field is achieved when the field is large enough, so that the simultaneous reduction in the drop of the phosphor field due to the emission rate of the carriers from the interface states can be compensated by the increase in the phosphor electric field provided by the rising voltage (B to C). As shown in Fig. 5(c) and (d), the ZnS:Mn TDEL device displays the steady-state field and a poor field clamping effect during the BC segment. The GaN:Eu device does not exhibit either an equivalent steady-state electric field or field clamping [Fig. 6(c)], probably due to a combination of phosphor material imperfections, dynamics of phosphor-insulator interface layers, transport irregularities related to defects in the band structure, etc.

The phosphor field relaxation begins once the applied pulse enters the segment C-D where the voltage is constant. It can be understood from the theoretical model that during C to D the ZnS:Mn TDEL device loses some of its internal field due to the transfer of charge across a relaxed electric field. A similar situation occurs for the GaN:Eu TDEL. The drop in the GaN:Eu phosphor electric field [Fig. 6(c)] is more rapid than for ZnS:Mn, possibly due to carrier transport characteristics in GaN. The rapid loss of electric field at constant applied voltage is certainly not a desirable feature of the device and more analysis is needed to understand and eliminate this problem. Furthermore, the polarity of the field decreases and reverses the sign with the fall of the bias voltage. The charge transferred during the voltage pulse creates an electric field that is in opposite polarity to that set in the device by the applied pulse. The reverse in polarity in the electric field is observed in both ZnS:Mn [Fig. 5(c)] and GaN:Eu [Fig. 6(c)] ACTDEL devices. The EL emission in both ZnS:Mn and Gan:Eu TDEL devices is observed at point B in the applied waveform when the phosphor breakdown occurs. The EL emission has a lifetime of $\sim$ 1 ms and $\sim$ 200 μs for ZnS:Mn and GaN:Eu TDEL devices, respectively.

2) External Charge–Voltage (Q–V) Analysis: External charge–voltage (Q–V) analysis is a classical characterization method employed for both TFEL and TDEL devices. Similar to the device steady-state time-varying characteristics, the Q–V is evaluated after a steady-state has been achieved. As shown in the main charge–voltage diagram of Fig. 3, an external Q–V loop progresses counterclockwise with time and one complete loop represents one whole cycle in the driving waveform. For the inset circuit diagram of Fig. 3, the ITO electrode is connected to the sense capacitor and the Al electrode is connected to the series resistor. Point A of the Q-V loop corresponds to the beginning of the applied voltage pulse. A negative value of charge is observed at point A, due to electron charge build-up (previously trapped charge) at the lower phosphor-insulator interface (adjacent to ITO bias electrode). This charge, the polarization charge, is left behind from the previous pulse of opposite polarity. The AB portion of the Q-V is from the rising edge of the applied waveform up to a level just below the device turn-on voltage.

It is important to note that two turn-on voltages are indicated instead of two threshold voltages in the main diagram of Fig. 3. The distinction between the turn-on voltage and the threshold voltage can be explained as follows. The turn-on voltage depends on the polarization charge, and hence on the magnitude of the $V_{\max}$ employed, whereas the threshold voltage is a constant value and does not depend upon $V_{\max}$. It is also proper to say that the threshold voltage is the turn-on voltage evaluated in the limit at which the polarization charge is zero. Thus, the TDEL device can possess different turn-on voltages depending on the applied maximum bias voltage but can have only one threshold voltage. Therefore, in practice, an effort should be made not to use the turn on voltage on occasions where threshold voltage is needed in device electrical characterization.

At B, the phosphor field clamps (in an ideal device) and an increase in the slope of the Q-V curve (increase in the total capacitance) is observed. The BC segment corresponds to the rising part of the applied waveform above the turn-on voltage (V_{to}) of the ACTDEL device. In the Q-V loop CD represents the portion of the applied waveform at a constant maximum voltage. The phosphor field decreases or relaxes due to the flow of charge under a constant voltage. The charge transported during this period is the relaxation charge. The total amount of charge during the segments BC and CD, the conduction charge, will contribute to the excitation of the luminescent centers within the phosphor. Segment DE is the falling edge of the applied voltage pulse. The segment EF corresponds to the zero bias voltage time duration. The leakage charge at EF is believed to be the charge released from the shallow states in the phosphor-insulator interface and from possible bulk traps within the phosphor defects. The remainder of the Q-V curve is similar to the above with the applied pulse being of opposite polarity.

With reference to the actual Q-V data collected for the ZnS:Mn TDEL device [Fig. 7(a)] the important features that were explained above are clearly seen. The barely open Q-V curve at 160 V shows that the device behaves almost as a capacitor throughout the voltage cycle. Thus, the polarization charge in the case of 160-V curve is close to zero, whereas once the voltage is increased to 170-V the curve opens dramatically and significant polarization charge is observed. Therefore, extending the previous explanation, we have found from the luminance–voltage plot that the threshold voltage (voltage at which polarization charge is zero) in the ZnS:Mn TDEL device is around 154 V. The experimental Q–V results for ZnS:Mn TDEL at 180-V shows a maximum charge of $\sim 3\ \mu\text{C/cm}^2$ coupled across the device. The TD layer on the TDEL is mainly responsible for the coupling of large amounts of charge across the device beyond the turn-on point. The ZnS shows a clear "knee" at the rising edge of the voltage pulse, as predicted by the theoretical analysis. The sharp opening of the Q–V curve above the threshold voltage indicates a nonleaky phosphor layer. It has been observed in Q–V plots that there is more conduction charge across the TDEL at lower modulation voltages when compared to ZnS:Mn TFEL (ZnS:Mn TDEL $\sim 0.08\ \mu\text{C/cm}^2\text{V}$ and ZnS:Mn TFEL $\sim 0.03\ \mu\text{C/cm}^2\text{V}$ at 180-V peak bias). This is a key advantage of the TDEL device structure. The sharp turn on of the ZnS TDEL device observed at 170 and 180 V can be ascribed to very strong charge trapping at the phosphor-dielectric interface. Also, the ZnS TDEL device shows extremely low leakage charge mainly due to excellent thin dielectric layers ($< 0.2\ \mu\text{C/cm}^2$ at 180 V).

The maturity of the ZnS as an electroluminescent phosphor clearly stands out in the comparison between ZnS and GaN [Fig. 7(b)] TDEL devices. The slope of the segment AB (rising pulse at subthreshold regime) in the ZnS TDEL is much less steep than in the GaN TDEL (ZnS:Mn $\sim 12\ \text{nF/cm}^2$ and GaN $\sim 21\ \text{nF/cm}^2$ at 180-V peak voltage). The steeper slope and the less prominent "knee" at point B in the GaN TDEL implies weak charge sourcing at the phosphor-insulator interface and charge transport across phosphor at subthreshold voltages, resulting in an inadequate shorting of the phosphor layer and only a weak field-clamping. It is desired to have GaN act as an insulator at subthreshold voltages rather than as a resistor parallel to the phosphor capacitive layer. Moreover, the GaN shows more leakage charge during the EF and AJ potions of the QV curve than the ZnS. This points out again the presence of leakage charge from the bulk traps within the GaN phosphor. Insufficiently populated interface trap density at the cathodic interfaces in the GaN device can explain the lack of field clamping observed in the curves at different applied voltage. Work is in progress to improve the insulating behavior of GaN under subthreshold bias while generating avalanching during above-threshold bias and in producing strong charge trapping at phosphor-dielectric interfaces.

3) Internal Charge–Phosphor Field (Q–F_p): The experimental external charge versus voltage (Q–V) plot (Fig. 7) provides vital information regarding the overall device performance. To understand the dynamics of charge across the phosphor layer we need to obtain the relationship between the internal charge and the phosphor field (F_p). There are reasons why the Q–V plot is not providing sufficient information in this aspect. In Fig. 7 the external charge actually corresponds to both external (total device) and internal (phosphor only) charges (for instance, segment A–B corresponds to both internal and external charge while segment B–C corresponds to external charge only). From a device understanding point of view, it is more interesting to analyze the charge across the phosphor

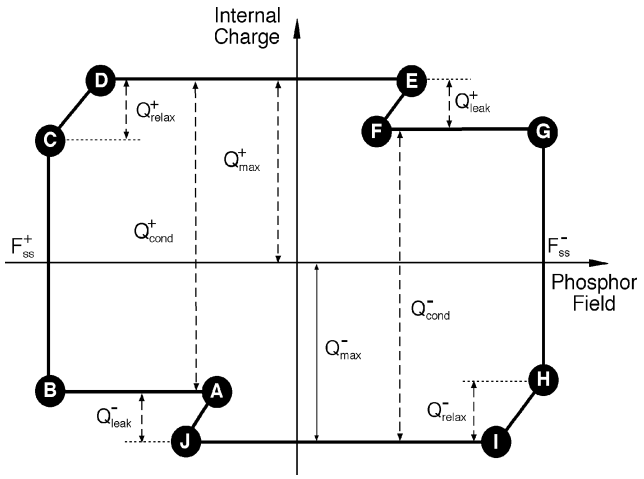

Fig. 8. Theoretical internal charge-phosphor field plot.

against the phosphor electric field than against the total device voltage (which is the case in Q–V).

The theoretical Q–F_p curve (Fig. 8) has been labeled A–J, similar to the Q–V curve (Fig. 3), to follow along with the applied voltage to the device. However, the Q–F_p plot traverses clockwise, whereas the Q–V progresses counter clockwise. The same charges (such as polarization charge, conduction charge and relaxation charge) that were present in the Q–V diagram are also present in the Q–F_p diagram. Starting from point A, where the device is at zero bias and a positive pulse is just applied, there will be a charge left behind from the previous opposite polarity pulse as discussed before in the case of Q–V curve. It can be seen that for fields below turn on (segments A–B), the phosphor electric field increases without any corresponding change in the internal charge. This is because the charge is thought to traverse through the phosphor layer only after the turn-on electric field has been reached. At point B, the device turns on. As explained before, the flow of trapped charge occurs simultaneously at turn on from the cathode biased interface toward the anode interface. With the applied voltage still increasing from B to C, the rising voltage compensates for the loss in the component of the phosphor electric field due to the motion of charge after turn on. Theoretically, this leads to a constant electric field across the phosphor during this time period. Therefore, from B to C the Q–F_p curve shows an increase in the charge at a constant electric field. The phosphor electric field reached at point B (turn on) is the maximum electric field that the phosphor will experience during the voltage pulse and will be constant during the segment B-C. Thus, it is named the *steady-state field* $F_{\rm ss}$. In theory, the steady-state field reached would be independent of the maximum applied voltage. This phenomenon is known as *field clamping*.

From point C to D, the applied voltage is constant at its peak value. The phosphor electric field is seen to be relaxed due to the charge flow across the phosphor and begins to drop. The charge traversed during this potion is termed *relaxation charge*. From D to E, the voltage falls, and the phosphor field drops and reverses polarity due to the residual charge that transferred from the cathode to the anode during the pulse. There is no charge flow during this segment of the applied pulse, thus the section DE remains horizontal in Fig. 8. Furthermore, it is seen from

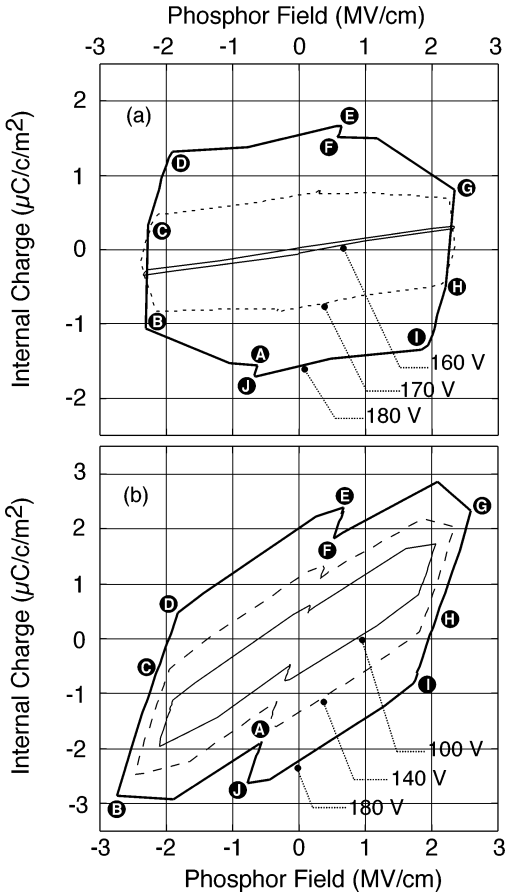

Fig. 9. Internal charge–phosphor field plots for TDEL devices: (a) ZnS:Mn and (b) GaN:Eu.

the Q-F_p curve that the net charge is traversed across the phosphor layer only during the segments BC and CD. The net charge flow during this period is termed the *conduction charge*. During the duration when the applied voltage is at zero (E-F) there will be a leakage of the charge transferred from the positive pulse. The decrease in the charge due to leakage will result in a corresponding reduction in the phosphor electric field and the lost charge during E-F is called the *leakage charge*. In this fashion, during the negative voltage pulse the charge flow occurs toward opposite directions from the positive pulse but illustrates the same features such as steady-state field, conduction charge and relaxation charge.

The experimental Q-F_p curves for the ZnS:Mn TDEL [Fig. 9(a)] are similar to those found in the literature [30] for ZnS:Mn TFELs. This indicates that the ZnS:Mn phosphor in TDEL undergoes similar charge distribution effects to a TFEL, which implies that in terms of device physics point of view the TDEL device is similar to a TFEL. The labels in Fig. 9(a) correspond to the same points in the ideal Q-F_p diagram of Fig. 8. One observation is that the segments A-B, D-E, F-G, and I-J of the actual device exhibit a "knee" when compared to the ideal device (Fig. 8). This effect is likely to be caused by the piezoelectric relaxation of the TD layer. Another important device parameter observable in Fig. 9(a) is the steady-state field $F_{\rm ss}$ of $\sim$ 2.5 MV/cm, which is constant or nearly constant during the rising portion of the applied voltage above turn on.

The TDEL F_{ss} is nearly twice that which is obtained in TFEL devices [31] under same biasing conditions ($\sim$ 1.5 MV/cm). The field clamping effect above threshold in the device is seen at different modulation voltages. Also, the leakage charge shown in the ZnS TDEL is extremely low ($\sim 0.2\ \mu C/cm^2$).

Similarly, the Q–F_p plot for GaN:Eu TDEL device [Fig. 9(b)] is labeled (to the best of our understanding) to correlate with Fig. 8. Again, the "knee" due to the piezo–electric relaxation of the TD layer is present in [Fig. 9(b)]. Furthermore, the distinctive knee observed at point C in the ideal device (Fig. 8) is not observed in the actual device Fig. 9(b). The lack of hot electron transport at phosphor breakdown and "warm" carrier transfer across the phosphor throughout the segments B–C and (most of) C–D of the applied waveform could be causing this effect. For the GaN:Eu TDEL devices [Fig. 9(b)] neither field clamping nor steady-state fields are observed . This is most likely due to the fact that insulator capacitance cannot be calculated with great accuracy from the current Q–V plots. On the other hand, very poor charge trapping at the phosphor–insulator interface and leakage within the phosphor might be preventing the field clamping and steady-state field from occurring in the GaN:Eu TDEL.

V. Summary and Conclusion

In summary, high brightness EL devices with ZnS:Mn and GaN:Eu inorganic phosphors have been realized using high-κ PZT sol-gel based TD layers. The brightness improvement in GaN:Eu TDEL device is more than $10\times$ ($\sim 450\ cd/m^2$). The low porosity of the TD layer has in turn reduced the diffuse reflection, which when pigmented, demonstrated a very high contrast. The PZT composite TD layer also has provided significantly high charge transfer ($> 3\ \mu C/cm^2$) across the devices. Furthermore, since the PZT film has excellent field uniformity for such a TD its use allows the electrical characteristics of the phosphor material to be observed. TDEL devices function electrically very similarly to the TFEL devices despite the physical asymmetry. In conclusion, these results indicate that three critical display device requirements can be achieved in the TDEL device approach: a) formation on standard glass substrate; b) low reflectivity; and c) electric field homogeneity.

Acknowledgment

The authors thank D. Morton and E. Forsythe for technical discussions and encouragement.

References

[1] H. Yamamoto, "CRT phosphors and application to FED phosphors," in *SID Tech. Dig.*, 1996, pp. 165–168.

[2] Y. Yoshida, A. Ishizuka, and H. Makishima, "Present and future of vacuum fluorescent display and field emission display," *Mater. Chem. Phys.*, vol. 40, no. 4, pp. 267–272, 1995.

[3] P. E. Burrows, S. R. Forrest, and M. E. Thompson, "Prospects and applications for organic light-emitting devices," *Current Opinion Solid-State Mater. Sci.*, vol. 2, no. 2, pp. 236–243, 1997.

[4] J. C. Heikenfeld and A. J. Steckl, "Inorganic EL displays at the crossroads," *Info. Displ.*, pp. 20–15, Dec. 2003.

[5] Y. A. Ono, *Electroluminescent Displays*, Singapore: World Scientific, 1995.

[6] C. N. King, "Electroluminescent displays," *J. Vac. Sci. Technol. A, Vac. Surf. Films*, vol. 14, no. 3, pp. 1729–1735, 1996.

[7] K. E. Waldrip, J. S. Lewis, Q. Zhai, M. Puga–Lambers, M. R. Davidson, P. H. Holloway, and S. S. Sun, "Improved electroluminescence of ZnS:Mn thin films by codoping with potassium chlodire," *J. Appl. Phys.*, vol. 89, no. 3, pp. 1664–1670, 2001.

[8] X. Wu, D. Carkner, H. Hamada, I. Yoshida, M. Kutsukake, and K. Dantani, "Large-screen flat panel displays based on iFire's thick-dielectric electroluminescent (TDEL) technology," in *SID Tech. Dig.*, Seattle, WA, 2004, pp. 1146–1149.

[9] J. Heikenfeld and A. J. Steckl, "Electroluminescent devices on glass using a high temperature stable GaN-based phosphor and thick film dielectric," *IEEE Trans. Electron Devices*, vol. 49, no. 6, pp. 557–563, Jun. 2002.

[10] J. Heikenfeld, R. A. Jones, and A. J. Steckl, "Black dielectric electroluminescent 160×80 pixel display," in *SID Tech. Dig.*, Baltimore, MD, 2003, pp. 1098–1101.

[11] A. J. Steckl, J. Heikenfeld, M. J. Garter, R. H. Birkhahn, and D. S. Lee, "Rare earth doped gallium nitride–light emission from ultraviolet to infrared," *Comp. Semicond.*, vol. 6, pp. 48–52, 2000.

[12] A. J. Steckl, J. Heikenfeld, D. S. Lee, and M. J. Garter, "Multiple color capability from rare earth doped gallium nitride," *Mater. Sci. Eng. B*, vol. 81, no. 1/3, pp. 97–101, 2001.

[13] A. J. Steckl, J. C. Heikenfeld, D. S. Lee, M. J. Garter, C. C. Baker, Y. Wang, and R. Jones, "Rare-earth doped GaN: Growth, properties, and fabrication of electroluminescent devices," *IEEE J. Sel. Topics Quantum Electron.*, vol. 8, no. 4, pp. 749–766, Apr. 2002.

[14] M. F. Bulanyi, A. V. Kovalenko, and B. A. Polezhaev, "Electroluminescence behavior of ZnS:Mn^{2+} crystals," *Inorg. Mater.*, vol. 39, no. 3, pp. 222–224, 2003.

[15] N. T. Gurin, A. V. Shlyapin, and O. Y. Sabitov, "Variation of the electroluminescence spectra of ZnS:Mn thin-film emitters depending on the excitation level," *Tech. Phys. Lett.*, vol. 28, no. 8, pp. 631–634, 2002.

[16] P. Visschere, K. Neyts, D. Corlatan, J. Van den Bossche, C. Barthou, P. Benalloul, and J. Benoit, "Analysis of the luminescent decay of ZnS:Mn electroluminescent thin films," *J. Lumin.*, vol. 65, pp. 211–219, 1995.

[17] R. A. Dorey, S. B. Stringfellow, and R. W. Whatmore, "Effect of sintering aid and repeated sol infiltrations on the dielectric and piezoelectric properties of a PZT composite thick film," *J. Eur. Ceram. Soc.*, vol. 22, pp. 2921–2926, 2002.

[18] J. F. Wager and P. D. Keir, "Electrical characterization of thin film electroluminescent devices," *Annu. Rev. Mater. Sci.*, vol. 27, pp. 223–248, 1997.

[19] E. Bringuier, "Charge transfer in ZnS–type electroluminescence," *J. Appl. Phys.*, vol. 66, no. 3, pp. 1314–1325, 1989.

[20] ——, "Electron multiplication in ZnS-type electroluminescent devices," *J. Appl. Phys.*, vol. 67, no. 11, pp. 7040–7044, 1990.

[21] A. N. Krasnov and P. G. Hofstra, "Growth, characterization and modeling of alternating current thin-film electroluminescent devices," *Prog. Cryst. Growth Charact. Mat.*, vol. 42, pp. 65–164, 2001.

[22] A. N. Krasnov, "Alternating-current thin-film electroluminescent devices: Effect of fabrication conditions on aging and failure defect formation," *Prog. Crys. Grwth. Charact. Mat.*, vol. 37, pp. 123–167, 1998.

[23] W. E. Howard, "The importance of dielectric properties in a thin-film electroluminescent device," *IEEE Trans. Electron Devices*, vol. 24, no. 7, pp. 903–908, Jul. 1977.

[24] F. Williams, "High field electroluminescence," *J. Lumin.*, vol. 23, pp. 1–16, 1981.

[25] D. Theis, "Application of thin film electroluminescent devices," *J. Lumin.*, vol. 23, pp. 191–207, 1981.

[26] M. Dur, S. M. Goodnick, R. Redmer, M. Reigrotzki, N. Fitzer, and M. Stadele, "First principle modeling of high field transport in wide bandgap materials," *Phys. B*, vol. 272, pp. 295–298, 1999.

[27] A. J. Steckl, M. Garter, D. S. Lee, J. Heikenfeld, and R. Birkhahn, "Blue electroluminescence from Tm-doped GaN light emitting devices," *Appl. Phys. Lett.*, vol. 75, pp. 2184–2186, 1999.

[28] J. Heikenfeld, M. Garter, D. S. Lee, R. Birkhahn, and A. J. Steckl, "Red light emission by photoluminescence and electroluminescence from Eu-doped GaN," *App. Phys. Lett.*, vol. 75, no. 9, pp. 1189–1191, 1999.

[29] C. B. Sawyer and C. H. Tower, "Rochelle salt as a dielectric," *Phys. Rev.*, vol. 35, pp. 269–273, 1930.

[30] A. Abu-Dayah, S. Kobayashi, and J. F. Wager, "Internal charge-phosphor field characteristics of alternating-current thin-film electroluminescent devices," *Appl. Phys. Lett.*, vol. 62, no. 7, pp. 744–746, 1993.

[31] W. M. Ang, S. Pennathur, L. Pham, J. F. Wager, and S. M. Goodnick, "Evidence for band-to-band impact ionization in evaporated ZnS:Mn alternating current thin film electroluminescent devices," *J. Appl. Phys.*, vol. 77, no. 6, pp. 2719–2724, 1995.

Chanaka Munasinghe (S'01) received the B.S. degree (with high honors) in physics from the University of Cincinnati, Cincinnati, OH. He is currently pursuing the Ph.D. degree in electrical engineering at the University of Cincinnati. In his doctoral study, he is focusing on GaN:RE TD electroluminescent device development and optimization. His study has led toward optimization of GaN:RE phosphor material using a novel interrupted growth epitaxy technique and $> 25\times$ device luminance improvements.

Mr. Munasinghe is a member of the American Physical Society, the Sigma Pi Sigma Physics Honor Society, and the Society for Information Display.

Jason Heikenfeld (M'01) received the B.S. and Ph.D. degrees from the University of Cincinnati, Cincinnati, OH, in 1998 and 2001, respectively. His major was in electrical engineering with minors in both photonics and physics. His doctoral study was supported by the University of Cincinnati Distinguished Graduate Assistantship. His doctoral research concentrated on novel inorganic electroluminescent display devices based on rare-earth-doped GaN.

He is now a Research Scientist at Extreme Photonix Corporation, Cincinnati, OH. His main duties at Extreme Photonix involve leading the development of electroluminescent devices for flat panel displays. He has authored and coauthored more than 20 publications in refereed journals, conference proceedings, and a book chapter. He is an inventor on three pending U.S. patents.

Dr. Heikenfeld is a member of the Institute for Electrical and Electronics Engineers, the Society for Information Display, the Materials Research Society, and the American Society for Engineering Education.

Robert Dorey received the Ph.D. degree from the University of Surrey, Surrey, U.K., in 2000.

In July 2003, he was awarded a highly prestigious five-year Royal Academy of Engineering/Engineering Physical Sciences Research Council post-graduate research fellowship. He is currently a lecturer at Cranfield University, Cranfield, U.K., where he is leading the group developing low-temperature microscale freeform fabrication technologies for producing functional ceramic devices.

Roger Whatmore (M'01) received the Ph.D. degree from Cambridge University, Cambridge, U.K., in 1977.

He spent nearly 20 years working with the GEC Marconi (formerly Plessey) Research Laboratories, Caswell, U.K. on the development and exploitation of ferroelectric materials in a wide range of electronic devices, particularly sensors and actuators, for which work he was awarded GEC's Nelson Gold Medal in 1993. In October 1994, he took the Royal Academy of Engineering Chair in Engineering Nanotechnology at Cranfield University, where he leads a group developing the use of ferroelectrics in microsystems and nanotechnology. He has published over 200 papers and 30 patents in the field.

Dr. Whatmore is a Fellow of the Royal Academy of Engineering and a Fellow of the Institute of Materials, Minerals and Mining who, in 2003, awarded him the Griffith Medal for Excellence in Materials Science.

Jeffrey P. Bender received the B.S., M.S., and Ph.D. degrees in electrical engineering from Oregon State University, Eugene, in 1998, 2000, and 2003, respectively. His academic research work was concerned with thin-film electroluminescence devices, including investigation of novel phosphor materials, low-temperature processing on plastic substrates, electro-optical device characterization, and computer simulation of device electrical properties.

He currently works in technology development for Intel Corporation, Aloha, Oregon.

John F. Wager (SM'78) received the B.S. degree in engineering physics from Oregon State University (OSU), Eugene, in 1977, and the M.S. and Ph.D. degrees in electrical engineering from Colorado State University, Fort Collins, in 1978 and 1981.

From 1982 to 1984, he worked at Hughes Research Laboratories where he was involved in the development of compound semiconductor devices for high-speed and optoelectronic applications. He joined the School of Electrical Engineering and Computer Science at OSU in 1984 where he is currently a Professor. His specialization and research focus is in the area of solid-state materials and devices. Recent research thrusts include thin-film electroluminescent devices for flat-panel displays, transparent electronics, printed electronics, and photovoltaics.

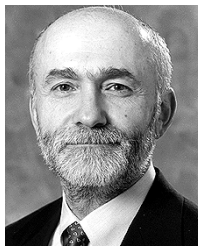

Andrew J. Steckl (S'70–M'73–SM'79–F'99) received the B.S.E. degree in electrical engineering from Princeton University, Princeton, NJ, in 1968, and the M.Sc. and Ph.D. degrees from the University of Rochester, Rochester, NY, in 1970 and 1973, respectively.

In 1972, he joined the Honeywell Radiation Center, Lexington, MA, as a Senior Research Engineer, where he worked on new concepts and devices in the area of infrared detection. In 1973, he joined the Technical Staff of the Electronics Research Division of Rockwell International, Anaheim, CA. At Rockwell he was primarily involved in research on charge coupled devices. In 1976, he joined the Electrical, Computer and Systems Engineering Department at Rensselaer Polytechnic Institute in Troy, NY, where he developed a research program in microfabrication of Si devices. In 1981, he founded the Center for Integrated Electronics, a multidisciplinary academic center focused on VLSI research and teaching, and served as its director until 1986. In 1988, he joined the Electrical and Computer Engineering Department, University of Cincinnati as Ohio Eminent Scholar and Gieringer Professor of Solid-State Microelectronics. At Cincinnati he has built the Nanoelectronics Laboratory with research activities in semiconductor materials and devices for photonics. Current activities include GaN MBE growth, rare-earth-doped luminescent devices, hybrid inorganic/organic materials and devices for flat panel displays and solid state lighting. His research has resulted in 330 publications and over 350 conference and seminar presentations.